Research Square

Preprints are preliminary reports that have not undergone peer review.
They should not be considered conclusive, used to inform clinical practice,
or referenced by the media as validated information.

Radical-mediated 1,2-nitrogen migration from silicon to carbon through iron LMCT photochemistry

Yi Jin
jinyi@ynu.edu.cn
Yunnan University
YingYing Yang
Yunnan University
Hao Jin
Yunnan University
Siyu Wang
Yunnan University
Dijie Li
Yunnan University
Yingcheng Wang
Yunnan University
Zhihui Shao
Yunnan University
Pengcheng Gao
Rutgers University https://orcid.org/0000-0003-4266-0616

Article

Keywords:

Posted Date: November 4th, 2026

DOI: https://doi.org/10.21203/rs.3.rs-11177005/v1

License: This work is licensed under a Creative Commons Attribution 4.0 International License.
Read Full License

Additional Declarations: There is **NO** Competing Interest.

Radical-mediated 1,2-nitrogen migration from silicon to carbon through iron LMCT photochemistry

Yingying Yang,[1] Hao Jin,[1] Siyu Wang,[1] Dijie Li,[1] Yingcheng Wang,[1] Zhihui Shao, [1] Pengcheng Gao*,[2] and Yi Jin*,[1]

Affiliations

[1] Key Laboratory of Medicinal Chemistry for Natural Resource, Ministry of Education; Yunnan Provincial Center for Research & Development of Natural Products; School of Pharmacy, Yunnan University, Kunming, 650091, P. R. China.

[2] School of Pharmaceutical Science and Yunnan Key Laboratory of Pharmacology for Natural Products and College of Modern Biomedical Industry, Kunming Medical University, Kunming, Yunnan 650500, China

*Corresponding author. Email: pg459@scarletmail.rutgers.edu (P.G.); jinyi@ynu.edu.cn (Y.J.)

Abstract: Radical-mediated migration provides an unconventional approach to reorganizing C–N connectivity, yet known transformations have largely relied on nitrogen migration from carbon-, nitrogen- or oxygen-linked precursors. Here we report the discovery of a visible-light-driven, $FeCl_3$-catalysed reaction that reveals silicon as a distinct origin for nitrogen translocation. Mechanistic experiments and computational studies support a pathway in which an Si–N intermediate is generated in situ and undergoes 1,2-nitrogen migration from silicon to carbon, ultimately forming an imine intermediate. This intermediate serves as a versatile branching point for subsequent bond formation, enabling modular incorporation of N-, O-, S- and Se-based nucleophiles, as well as intramolecular cyclization and cascade annulation. Variation of the nitrogen-containing component, hydrosilane and trapping partner provides access to a broad range of difunctionalized products and heterocyclic frameworks. Experimental mechanistic studies and DFT calculations collectively support a direct intramolecular Si-to-C nitrogen migration through a three-membered Si–C–N transition state. These findings expand the bonding environments from which radical nitrogen migration can originate and establish Si–N bonds as a potential entry point for nitrogen translocation and complexity-generating synthesis.

Main Text: Migration and rearrangement reactions provide a powerful means of molecular reorganization, rapidly generating structural complexity through the controlled cleavage and formation of chemical bonds.[1] Whereas classical rearrangements predominantly proceed through ionic pathways, the renaissance of radical chemistry has revealed distinct opportunities for functional-group translocation.[2-4] Unlike ionic processes, which often depend on the generation and stabilization of charged intermediates, radical rearrangements can reorganize otherwise inert bonds through unconventional reaction trajectories, alleviating constraints associated with bond dissociation energies and spatial proximity.[5,6] This reactivity has enabled the migration of aryl, cyano, alkenyl and alkynyl groups, as well as heteroatom-containing functionalities involving halogens, boron and silicon, establishing radical migration as a versatile strategy for molecular editing and skeletal reorganization.[6]

Despite the prevalence of nitrogen-containing functionalities in bioactive molecules and synthetic intermediates, radical-mediated nitrogen migration remains comparatively underdeveloped. Nature provides an early blueprint for such reactivity: Barker and co-workers first characterized lysine 2,3-aminomutase in 1970, establishing the enzymatic interconversion of α- and β-lysine,[7] while Frey and co-workers subsequently provided direct EPR evidence for organic radical intermediates in this rearrangement in 1992.[8] More recently, Yang, Liu and co-workers engineered non-haem iron enzymes to enable asymmetric 1,3-nitrogen migration through hydrogen-atom transfer followed by stereoselective radical rebound.[9] Beyond enzymatic systems, radical nitrogen migration has also been realized through synthetic approaches. In 1990, Frey and co-workers reported an AIBN-initiated and radical-mediated 1,2-imino rearrangement,[10] whereas subsequent metal-free strategies developed by Zhu and co-workers in 2016 and Han, Jiao and co-workers in 2021 employed externally generated azidyl or fluoroalkyl radicals to initiate nitrogen translocation within suitably designed unsaturated substrates.[11,12] In addition, transition-metal catalysis has substantially broadened the mechanistic repertoire available for radical mediated-nitrogen migration. In 2017, Wang and co-workers developed a Cu-catalysed radical 1,3-nitrogen shift from $C(sp^3)$ to $C(sp^2)$ through an unusual 4-exo-trig cyclization of an N-centred radical onto an aryl ring.[13] In 2022, Meggers and co-workers developed a Ru-catalysed stereocontrolled 1,3-nitrogen migration from oxygen to carbon through N–O bond cleavage and nitrenoid-mediated radical relay, and subsequently extended this strategy to enantioselective olefin oxyamination in 2023.[14,15] More recently, Tang and co-workers established a Ni-catalysed $C(sp^3)$-to-$C(sp^3)$ 1,2-nitrogen migration in 2024 through an extrusion–readdition manifold involving C–N bond fragmentation and radical readdition. This reactivity was subsequently extended by their group and independently by Huang and co-workers to asymmetric migratory cross-coupling in 2025.[16-18] Furthermore, photochemical activation has provided a complementary platform for radical mediated-nitrogen migration. In 2024, Han and co-workers developed an Ir-photoredox-catalysed remote imino-N translocation through radical addition, cyclization and N–N bond fragmentation.[19] In 2025, Zhang and co-workers established a biomimetic photoredox 1,2-amino migration through a radical addition–3-exo-trig cyclization–ring-opening sequence,[20] while Huang and co-workers developed a visible-light energy-transfer-catalysed amino-group migration through a triplet-diradical rearrangement.[21] Collectively, these advances demonstrate that radical nitrogen translocation can operate over different migration distances and from diverse bonding environments, including C–N, N–N and N–O linkages. Yet, whether other element–nitrogen bonds can serve as viable origins for radical nitrogen migration remains largely unexplored.

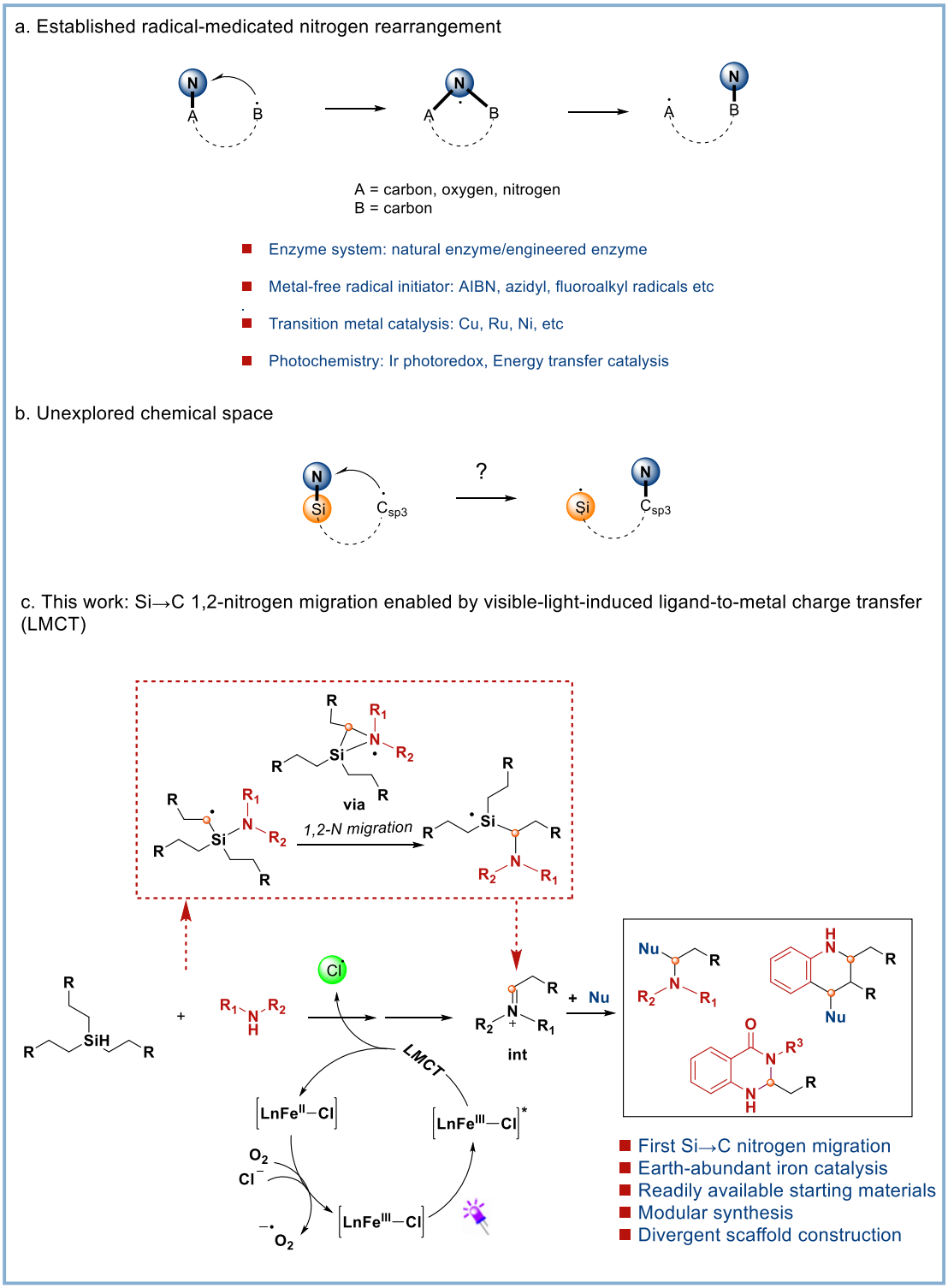
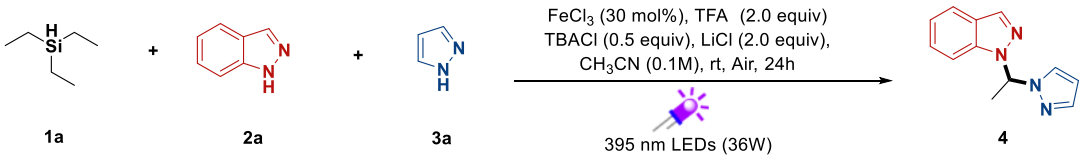


Fig. 1. Context of this work. a Established radical-mediated nitrogen rearrangement. b Unexplored chemical space. c. This work: Si→C 1,2-nitrogen migration enabled by visible-light-induced ligand-to-metal charge transfer (LMCT).

Here, we report the discovery of a visible-light-driven, $FeCl_3$-catalysed cascade reaction that enables the modular assembly of diverse nitrogen-containing scaffolds and heterocycles from readily available components. The unexpected connectivity of the products prompted us to

investigate the origin of the newly formed C–N bond. Mechanistic experiments and computational studies support an unusual pathway involving the in situ formation of an Si–N intermediate, subsequent 1,2-nitrogen migration from silicon to carbon, and formation of a key imine intermediate. This imine provides a versatile branching point for divergent cascade reactions, allowing different reaction components to be modularly assembled into structurally diverse products. The transformation features operational simplicity, broad functional-group tolerance and extensive substrate scope. Viewed through this mechanistic framework, the Si–N bond emerges as a potential new entry point for radical nitrogen migration, expanding the scope of nitrogen-translocation chemistry and offering a complementary strategy for molecular reorganization and complexity generation.

Table 1. Optimization of the three-component difunctionalization of triethylsilane.[a, b]



Entry	Catalyst	Acid	Additive	Chloride additive	Solvent	Light source	Yield of **4** (%)[b]
1	$FeCl_3$	TFA	TBACl	LiCl	CH_3CN	395 nm	80
2	$FeCl_2$	TFA	TBACl	LiCl	CH_3CN	395 nm	73
3	$Fe(OTf)_3$	TFA	TBACl	LiCl	CH_3CN	395 nm	71
4	$Fe(NO_3)_3{\cdot}9H_2O$	TFA	TBACl	LiCl	CH_3CN	395 nm	36
5	$FeCl_3$	TFAA	TBACl	LiCl	CH_3CN	395 nm	72
6	$FeCl_3$	CHF_2COOH	TBACl	LiCl	CH_3CN	395 nm	68
7	$FeCl_3$	TfOH	TBACl	LiCl	CH_3CN	395 nm	59
8	$FeCl_3$	HCl	TBACl	LiCl	CH_3CN	395 nm	79
9	$FeCl_3$	AcOH	TBACl	LiCl	CH_3CN	395 nm	19
10	$FeCl_3$	TFA	TBAF	LiCl	CH_3CN	395 nm	78
11	$FeCl_3$	TFA	$TBABF_4$	LiCl	CH_3CN	395 nm	76
12	$FeCl_3$	TFA	TBABr	LiCl	CH_3CN	395 nm	61
13	$FeCl_3$	TFA	TBAI	LiCl	CH_3CN	395 nm	58
14	$FeCl_3$	TFA	$TBAPF_6$	LiCl	CH_3CN	395 nm	57
15	$FeCl_3$	TFA	TBACl	LiCl	DCE	395 nm	62
16	$FeCl_3$	TFA	TBACl	LiCl	EtOAc	395 nm	41
17	$FeCl_3$	TFA	TBACl	LiCl	Toluene	395 nm	N.D.
18	$FeCl_3$	TFA	TBACl	LiCl	DMSO	395 nm	N.D.
19	$FeCl_3$	TFA	TBACl	LiCl	EtOH	395 nm	N.D.
20	$FeCl_3$	TFA	TBACl	LiCl	CH_3CN	365 nm	65
21	$FeCl_3$	TFA	TBACl	LiCl	CH_3CN	460 nm	36
22	—	TFA	TBACl	LiCl	CH_3CN	395 nm	N.D.
23	$FeCl_3$	—	TBACl	LiCl	CH_3CN	395 nm	trace
24	$FeCl_3$	TFA	—	LiCl	CH_3CN	395 nm	68
25	$FeCl_3$	TFA	TBACl	—	CH_3CN	395 nm	72
26	$FeCl_3$	TFA	TBACl	LiCl	CH_3CN	in dark	N.D.

[a]Conditions: **1a** (4.0 equiv), **2a** (1.0 equiv, 0.2 mmol), **3a** (2.0 equiv) $FeCl_3$ (30 mol%), TFA (2.0 equiv), TBACl (0.5 equiv), LiCl (2.0 equiv), CH_3CN (0.1 M), 24 h. [b]Yields were determined by analysis of the crude ^1H NMR spectra using CH_2Br_2 as an internal standard. N.D. = not detected.

Reaction Discovery and Optimization: Inspired by the ability of $FeCl_3$ photochemistry to activate hydrosilanes through ligand-to-metal charge transfer (LMCT) and subsequent hydrogen-atom transfer (HAT), we envisioned that hydrosilanes and N–H compounds could generate Si–N

intermediates in situ under visible-light irradiation. We reasoned that further radical activation of these Si–N species might provide an opportunity to explore previously unknown nitrogen translocation from silicon, with an external nucleophile serving to intercept the resulting reactive intermediates. On this basis, we selected triethylsilane, indazole and pyrazole as model components to investigate this potential Si–N rearrangement chemistry. Systematic evaluation of the reaction parameters identified conditions under which product **4** was obtained in 80% yield upon irradiation with 395-nm LEDs, using $FeCl_3$ as the catalyst, TFA as the acid additive, TBACl and LiCl as chloride additives, and MeCN as the solvent (Table 1, entry 1). The iron source had a notable influence on reaction efficiency: $FeCl_2$ and $Fe(OTf)_3$ remained competent, whereas $Fe(NO_3)_3 \cdot 9H_2O$ was substantially less effective (Table 1, entries 2–4). The reaction was also sensitive to the Brønsted acid, with several strong acids supporting efficient product formation, whereas the weaker AcOH led to a pronounced decrease in yield (Table 1, entries 5–9). Evaluation of tetraalkylammonium additives revealed a preference for chloride-containing conditions, although fluoride- and tetrafluoroborate-based salts also retained appreciable reactivity (Table 1, entries 11–14). The reaction efficiency was further influenced by the reaction medium and irradiation wavelength. MeCN proved optimal, with DCE remaining effective and EtOAc giving a diminished yield, whereas no detectable product was observed in toluene, DMSO or EtOH (Table 1, entries 16–19). Irradiation at either 365 or 460 nm instead of 395 nm also resulted in decreased yields (Table 1, entries 20–21). Importantly, control experiments established that both $FeCl_3$ and light were essential for productive reactivity, consistent with a photochemically initiated iron-catalysed process. Omission of TFA afforded only trace product, whereas removal of either TBACl or LiCl decreased, but did not completely suppress, product formation (Table 1, entries 22–26). Together, these studies established $FeCl_3$, 395-nm irradiation, a strongly acidic medium and chloride additives as the key reaction parameters for efficient formation of the nitrogen-translocation product.

Substrate Scope. With the optimized conditions in hand, we investigated the generality and modularity of the transformation by systematically varying the nitrogen-containing substrate and nucleophilic trapping partner (Fig. 2). We first examined the nitrogen-containing component using triethylsilane and a representative nitrogen nucleophile as the common reaction partners. Parent indazole underwent the transformation efficiently to afford **4** in 82% yield, while alkyl- and alkoxy-substituted derivatives were also well tolerated, furnishing **5**–**8** in good yields. Halogenated substrates remained competent, albeit with somewhat diminished efficiency in certain cases, as exemplified by chloro-substituted product **9**. The reaction was not restricted to simple indazole derivatives, as more structurally elaborate fused N-heterocycles also participated to provide **10**–**15**. Notably, potentially sensitive functionalities, including epoxide, hydroxy and ester groups, were retained under the reaction conditions, illustrating the functional-group compatibility of the transformation. Beyond heteroaromatic substrates, aromatic, aliphatic and cyclic amide derivatives were also competent, furnishing **16**–**21** and demonstrating that the reaction can accommodate structurally and electronically distinct nitrogen-containing components.

We next examined the scope of the nucleophilic trapping partner. A range of structurally and electronically varied N-heterocycles, including azoles bearing alkyl, aryl, halide, ester and nitro substituents, participated effectively to furnish the corresponding C–N functionalized products **22**–**32**, generally in moderate to good yields. Both electron-rich and electron-deficient heterocycles were compatible, indicating considerable electronic flexibility in the trapping step. The structure of triazole-derived product **28** was unambiguously confirmed by single-crystal X-ray diffraction.

Importantly, the trapping process was not limited to nitrogen nucleophiles. Primary, secondary and cyclic alcohols afforded the corresponding C–O functionalized products **33**–**39**; the structurally more complex L-menthol was also compatible, providing **39** in 61% yield with a 5.2:1 diastereomeric ratio. Sulfur nucleophiles exhibited particularly broad structural tolerance, with a diverse range of aromatic and aliphatic thiols furnishing **40**–**62** in generally moderate to good yields while tolerating alkyl, halide, hydroxy, amide and fused-aryl functionalities. The structure of **51** was further confirmed by single-crystal X-ray diffraction. Selenium- and sulfonyl-based reaction partners further expanded the scope, affording **63** and **64**, respectively. Collectively, the compatibility of N-, O-, S- and Se-based trapping partners demonstrates the versatility of this reaction manifold, enabling divergent C–N, C–O, C–S and C–Se bond formation and highlighting the modular nature of the downstream trapping process.

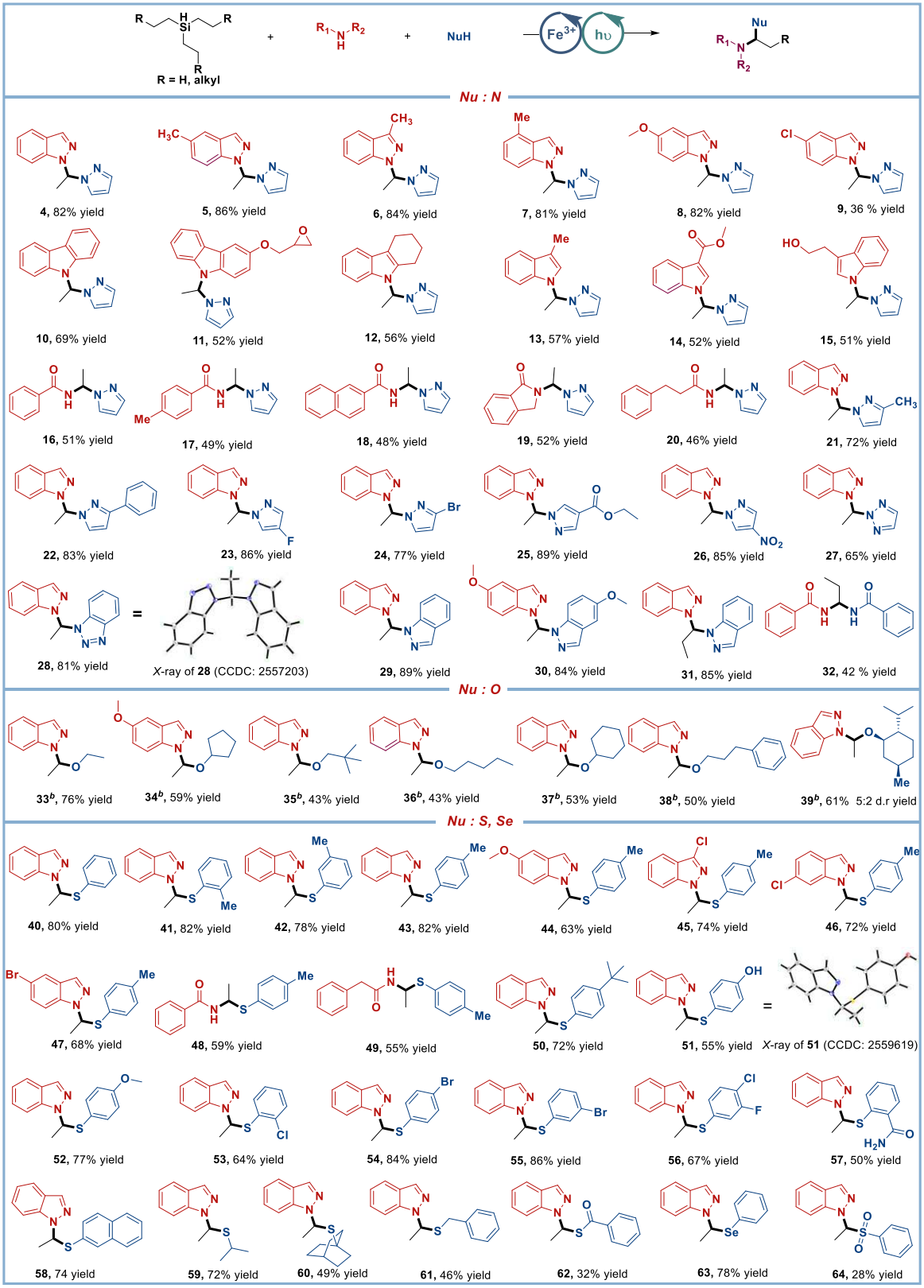


Fig. 2. [a]Conditions: **1** (4.0 equiv), **2** (1.0 equiv, 0.2 mmol), **3** (2.0 equiv) $FeCl_3$ (30 mol%), TFA (2.0 equiv), TBACl (0.5 equiv), LiCl (2.0 equiv), CH_3CN (0.1 M), 24-36 h. [b]Solvent: CH_3CN: DCE (1:1, 2.0mL, 0.1M).

We next explored whether the reaction could be extended from intermolecular trapping to intramolecular cyclization, providing direct access to more complex heterocyclic frameworks (Fig. 3). o-Aminobenzamide derivatives underwent the cascade process followed by intramolecular C–N bond formation to furnish 2,3-dihydroquinazolinones **65**–**74** in 45–80% yield, with diverse alkyl, benzyl and heteroarylmethyl substituents being tolerated. Intramolecular C–O bond formation was also feasible, affording oxygen-containing heterocycles **75** and **76**. These results suggest that the reactive intermediate generated following nitrogen translocation can also be intercepted intramolecularly, enabling direct heterocycle construction.

We next examined the hydrosilane component (Fig. 3). Hydrosilanes bearing alkyl groups with different chain lengths and substitution patterns participated in the transformation to furnish **77**–**88**, and could be combined with different nitrogen-containing substrates and trapping partners. Although increasing steric demand generally reduced the reaction efficiency, variation of the silicon-bound alkyl groups was directly reflected in the carbon skeleton of the products. Together with the broad scope of nitrogen-containing substrates and nucleophilic trapping partners, these results highlight the three-component modularity of the transformation.

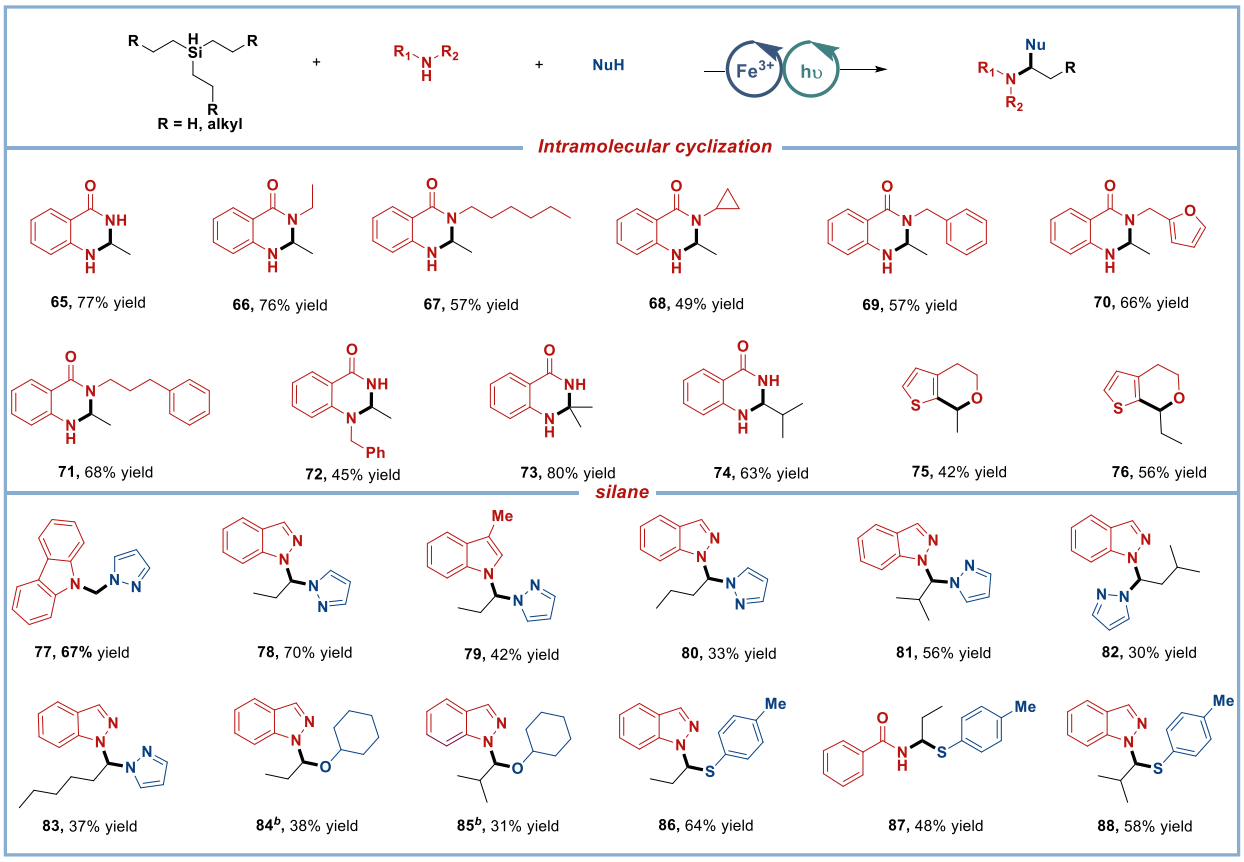


Fig. 3. [a]Conditions: **1** (4.0 equiv), **2** (1.0 equiv, 0.2 mmol), **3** (2.0 equiv) $FeCl_3$ (30 mol%), TFA (2.0 equiv), TBACl (0.5 equiv), LiCl (2.0 equiv), CH_3CN (0.1 M), 24-36 h. [b]Solvent: CH_3CN: DCE (1:1, 2.0mL, 0.1M).

We further explored whether the substrate scope could be integrated with an aniline-based cascade annulation to rapidly increase molecular complexity (Fig. 4). Under reoptimized conditions, anilines, hydrosilanes and azole nucleophiles underwent the cascade reaction to furnish

polysubstituted tetrahydroquinolines **89**–**104** in 26–73% yield. Product **89** was obtained in 71% yield, and its structure was established by single-crystal X-ray diffraction. Considerable variation of the aniline component was tolerated, including alkyl, methoxy, chloro and ester substituents (**90**–**97**), while a naphthylamine derivative also participated efficiently to afford **98**. The nucleophilic trapping partner could likewise be varied across substituted pyrazoles, triazole and benzotriazole, providing **99**–**103**. Variation of the hydrosilane component was also feasible, although increased steric demand resulted in diminished efficiency, as exemplified by **104**, obtained in 26% yield. Taken together, these studies demonstrate that the transformation is not limited to a single three-component coupling, but instead provides a modular reaction manifold that can be diversified across the nitrogen-containing substrate, nucleophilic trapping partner and hydrosilane.

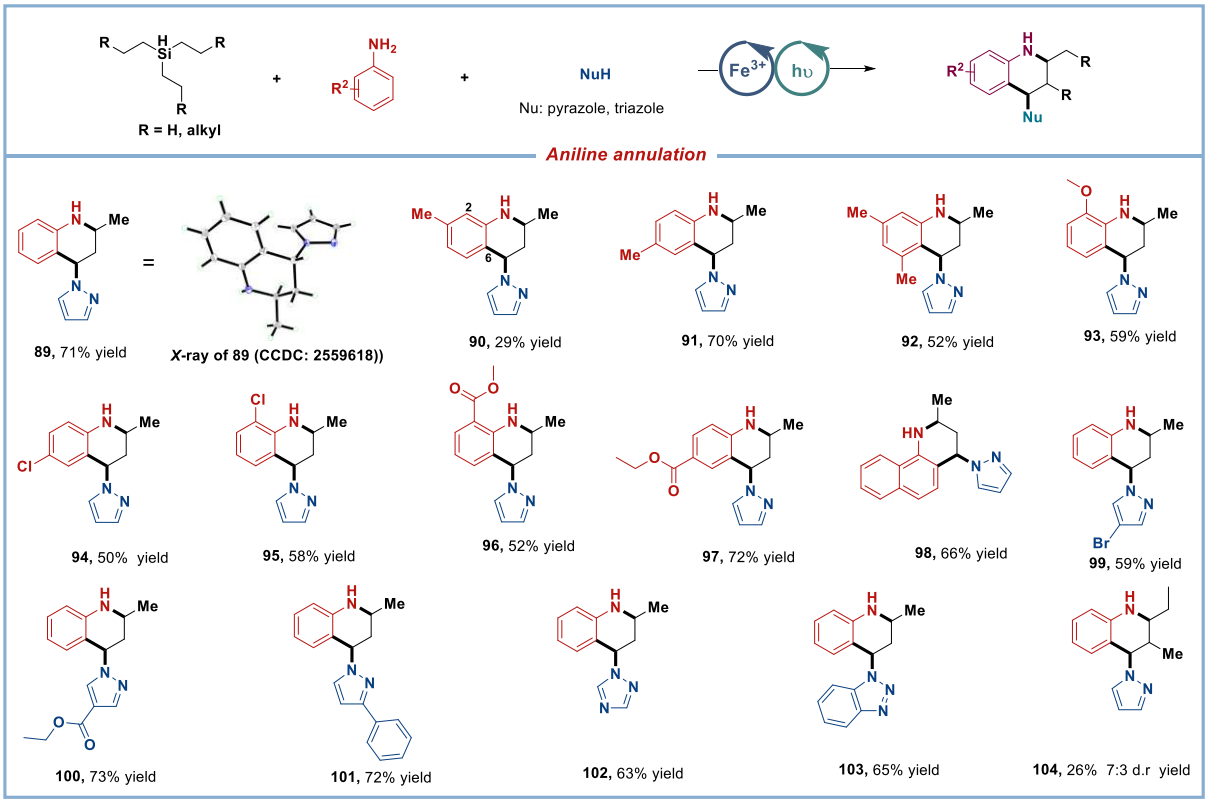


Fig. 4. [a]Conditions: **1** (4.0 equiv), **2** (1.0 equiv, 0.2 mmol), **3** (2.0 equiv) $FeCl_2$ (30 mol%), TFA (2.0 equiv), TBACl (0.5 equiv), LiCl (2.0 equiv), CH_3CN (0.1 M), 24-36 h.

Mechanistic Studies. To gain insight into the reaction pathway underlying the formation of these products, we conducted a series of mechanistic experiments (Fig. 5). We first probed the involvement of radical intermediates. Addition of TEMPO (4.0 equiv.) under the standard conditions almost completely suppressed formation of **4**, while HRMS analysis revealed an ion consistent with the triethylsilyl–TEMPO adduct **105** (Fig. 5a). In a complementary radical-probe experiment, a cyclopropyl-containing radical probe underwent ring opening under the reaction conditions, giving the silylated and chlorinated products **106** and **107**, respectively. Together, these observations support the involvement of radical species and are consistent with the generation of silyl and chlorine radicals under the reaction conditions.

We next sought evidence for the proposed Si–N intermediate that could precede nitrogen translocation. Independently prepared *N*-silylated carbazole **108** underwent the reaction with pyrazole to furnish **10** in 61% yield, demonstrating that an *N*-silylated species is chemically competent to enter the productive pathway (Fig. 5b). More directly, HRMS analysis of the standard reaction mixture revealed an ion consistent with *N*-silylated indazole **int-3** (calcd for $[M+H]^+$, *m/z* = 233.1469; found, 233.1461; Fig. 5c). The combination of in situ detection and intermediate-conversion experiments therefore provides support for the formation and productive involvement of *N*-silylated intermediates.

To distinguish an intramolecular Si-to-C nitrogen migration from pathways involving dissociation and intermolecular recombination of nitrogen- and carbon-derived fragments, we performed a crossover experiment using two independently prepared N-silylated intermediates bearing orthogonal nitrogen and carbon-fragment labels. An equimolar mixture of N-triethylsilyl indazole (A: **110**, N-tag: indazole, C-tag: Et) and N-tri-n-propylsilyl 5-methylindazole (B: **111**, N-tag: 5-Me-indazole, C-tag: n-Pr) was subjected to the photochemical reaction conditions in the presence of pyrazole. LC-HRMS analysis of the crude reaction mixture showed only the two matched products AA and BB, whereas neither crossover product AB nor BA was detected (Fig. 5d). The retention of the original N-silyl/carbon-fragment pairing strongly supports an intramolecular Si-to-C 1,2-nitrogen migration rather than an intermolecular nitrogen-transfer pathway.

Additional intermediate-conversion experiments were conducted to probe the cascade annulation of aniline substrates (Fig. 5b). A preformed N-vinylaniline underwent the reaction to furnish tetrahydroquinoline **104**, supporting its competence as an intermediate in the annulation pathway. Moreover, reaction of aniline and hydrosilane in the absence of the external azole afforded 4-anilino tetrahydroquinoline **109**, which was subsequently converted into **89** upon reaction with pyrazole. These stepwise experiments support a cascade sequence involving formation of an N-vinyl intermediate, cyclization to a tetrahydroquinoline intermediate, and subsequent incorporation of the external nucleophile.

Deuterium-labelling experiments provided further information on hydrogen-atom transfer during the reaction (Fig. S11). These observations are consistent with hydrogen-atom abstraction from the hydrosilane during the radical process. The roles of Fe(III) and chloride were examined independently (Table S12). $FeCl_3$ afforded **4** in 68% yield, whereas $Fe(OTf)_3$ in the absence of an added chloride source gave only trace product. Addition of LiCl to the $Fe(OTf)_3$ system restored the yield to 65%, demonstrating a pronounced dependence on chloride for efficient reactivity. Together with the radical-trapping experiments, these results are consistent with the involvement of chloride-ligated Fe(III) species and an Fe–Cl LMCT process capable of generating chlorine radicals upon photoexcitation. Consistent with a photochemically driven process, light on/off experiments showed that product formation largely ceased during dark periods and resumed upon irradiation (Fig. S12), indicating that continuous photoexcitation is required for efficient reaction turnover.

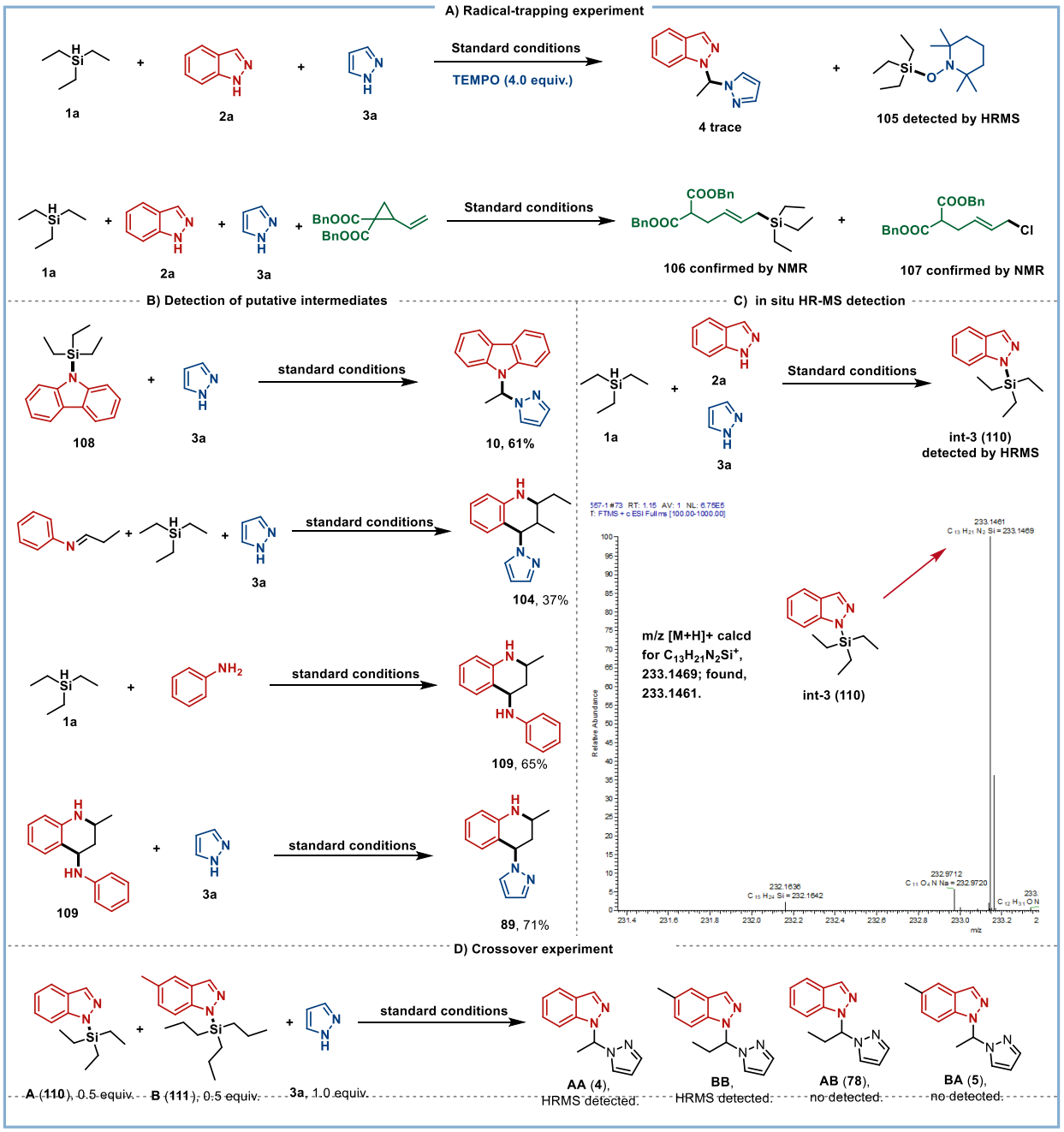


Fig. 5. Mechanistic studies.

Proposed mechanism. On the basis of the mechanistic experiments described above and relevant literature precedents, we propose the working mechanism depicted in Fig. 6. Upon photoirradiation, a chloride-ligated Fe(III) species undergoes Fe–Cl LMCT, generating a chlorine radical and an Fe(II) species.[22,23,24,25] The chlorine radical is proposed to abstract the Si–H hydrogen atom from hydrosilane **1** via hydrogen-atom transfer (HAT), affording silyl radical **int-1** and HCl.[23] The formation of a silicon-centred radical is consistent with the radical-trapping experiments and the detection of the corresponding silyl–TEMPO adduct. In parallel, nitrogen-containing substrate **2** may associate with an Fe(III) species to generate an Fe-associated nitrogen species **int-2**. Reaction of the silyl radical with the nitrogen-containing substrate ultimately furnishes *N*-silylated

intermediate **int-3**.[27,28] The involvement of **int-3** is also supported by its detection by HRMS and by the productive conversion of an independently prepared *N*-silylated intermediate under the reaction conditions. A chlorine radical then abstracts a hydrogen atom from the silicon-bound alkyl chain to generate the carbon-centred radical **int-4**.[24,26] Radical **int-4** is proposed to undergo an intramolecular 1,2-nitrogen migration from silicon to the adjacent carbon centre through a three-membered Si–C–N arrangement (**int-6**), furnishing silicon-centred radical **int-6**.[6] Oxidation of **int-6** by Fe(III) and/or an oxygen-derived oxidant affords the electrophilic silicon intermediate **int-7**. Subsequent C–Si bond fragmentation, accompanied by C=N bond formation, releases a silicon-containing fragment and generates the iminium intermediate **int-8**. In this way, the otherwise inert silicon-bound alkyl group is formally converted into an electrophilic carbon synthon.

For *N*-heterocyclic and amide-derived substrates (path a), iminium intermediate **int-8** is intercepted by *N*-, *O*-, *S*- or *Se*-based nucleophiles to afford the corresponding difunctionalized products. Aniline substrates follow a distinct cascade pathway (path b). The initially generated imine/enamine species **int-9**/**int-10** are proposed to undergo an intermolecular Povarov-type annulation to furnish 4-anilino tetrahydroquinoline **int-11**.[29] Subsequent nucleophilic substitution of the C4 anilino group by an external azole nucleophile affords the observed C4-functionalized tetrahydroquinolines. This sequence is consistent with the independent conversion experiments using the N-vinyl intermediate and the 4-anilino tetrahydroquinoline intermediate. For *o*-aminobenzamide substrates (path c), intramolecular attack of the ortho-amino group on the iminium carbon of **int-8** closes the six-membered ring, furnishing the corresponding 2,3-dihydroquinazolinones.

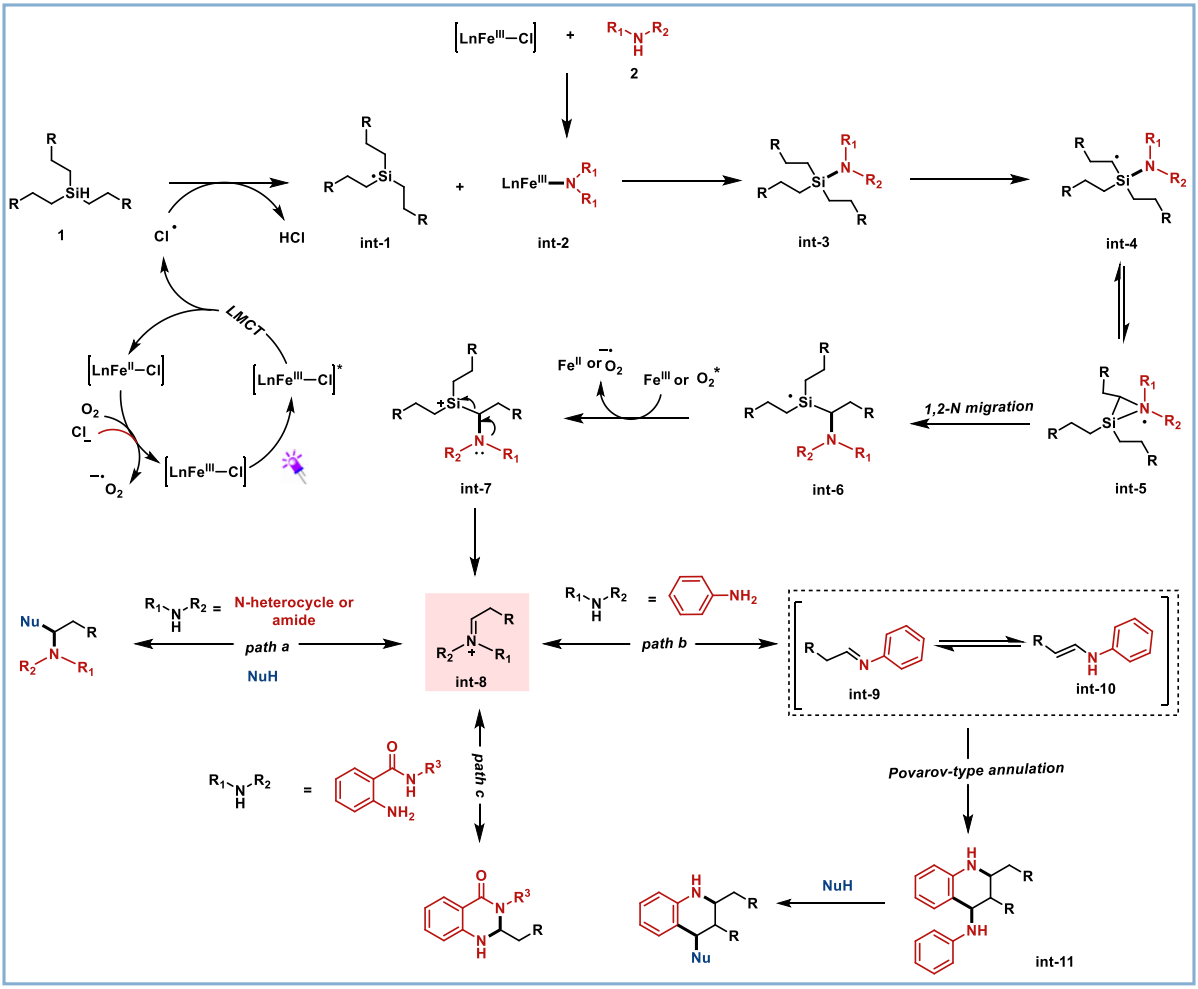


Fig. 6. Proposed mechanism.

Computational analysis. DFT calculations were used to evaluate the direct intramolecular int-4→int-6 Si-to-C nitrogen migration (Fig. 7). Geometry optimizations and vibrational analyses were performed at UωB97X-D/def2-SVP with SMD(MeCN), followed by UωB97X-D/def2-TZVPP/SMD(MeCN) single-point calculations. The migration proceeds through the three-membered Si–C–N transition state **TS-mig** with a Gibbs free-energy barrier of 14.2 kcal mol^{-1} relative to **int-4**, while **int-6** lies 8.7 kcal mol^{-1} below **int-4**. **TS-mig** has one imaginary frequency (−425 cm^{-1}), whose normal mode shows synchronous C–N bond formation and Si–N bond cleavage; the optimized Si–N, N–C and Si–C distances are 2.13, 1.91 and 1.92 Å, respectively, and IRC calculations connect i**nt-4**, **TS-mig** and **int-6**. Representative competing pathways are substantially higher in energy: N–Si bond dissociation (27.6 kcal mol^{-1}), direct C–Si bond cleavage (24.7 kcal mol^{-1}), and an intermolecular nitrogen-transfer model (25.1 kcal mol^{-1}). Consistent with bond reorganization, the spin density shifts from carbon in **int-4** (ρC = 0.85, ρSi = 0.05), becomes delocalized in **TS-mig** (ρC = 0.34, ρSi = 0.37, ρN = 0.18), and resides predominantly on silicon in **int-6** (ρC = 0.04, ρSi = 0.83). These results support a kinetically accessible and thermodynamically favourable intramolecular Si-to-C 1,2-nitrogen migration.

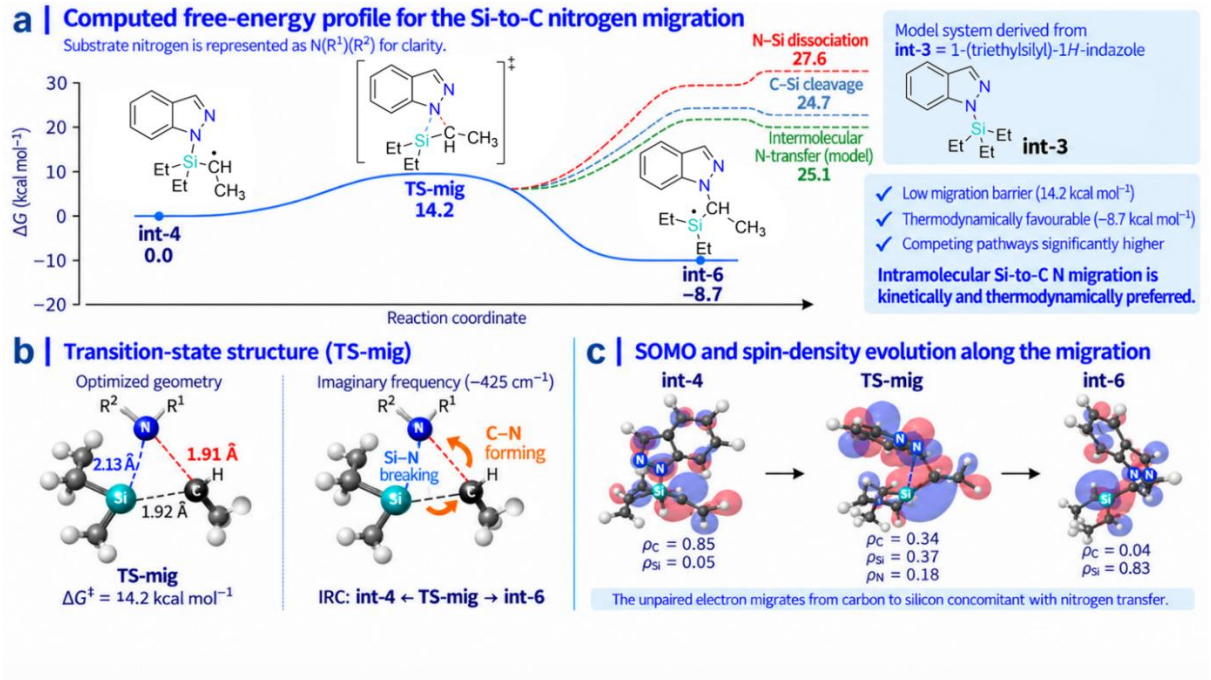


Fig. 7. DFT analysis of the intramolecular Si-to-C nitrogen migration. a, Computed free-energy profile for **int-4** → **TS-mig** → **int-6** and representative competing pathways. b, Optimized TS-mig structure showing synchronous C–N bond formation and Si–N bond cleavage. c, SOMO and spin-density evolution from a carbon-centred radical in int-4 to a silicon-centred radical in **int-6**.

Conclusions. In summary, we have uncovered a visible-light-driven, iron-catalysed cascade reaction that provides evidence for an unusual 1,2-nitrogen migration from silicon to carbon. Mechanistic experiments and computational studies support the in situ formation of an Si–N intermediate, followed by radical nitrogen translocation and conversion into a reactive imine intermediate. This mechanistic sequence provides a common basis for the diverse reactivity observed across the transformation: the resulting intermediate can be intercepted by N-, O-, S- and Se-based nucleophiles, engaged in intramolecular cyclization, or incorporated into cascade annulation processes to generate structurally diverse heterocycles. The modularity of the nitrogen-containing substrate, hydrosilane and trapping partner further enables substantial variation of the resulting molecular frameworks. DFT calculations further support a kinetically accessible and thermodynamically favourable intramolecular Si-to-C 1,2-nitrogen migration through a three-membered Si–C–N transition state, accompanied by translocation of the radical centre from carbon to silicon. More broadly, these findings suggest that element–nitrogen bonds beyond the established C–N, N–N and N–O linkages can participate in radical nitrogen translocation, identifying Si–N bonds as a potential platform for exploring new migration pathways. We anticipate that extending this principle to other element–nitrogen bonds may provide opportunities for discovering distinct modes of skeletal reorganization and complexity-generating synthesis.

References

1. Rojas, C. M. *Molecular Rearrangements in Organic Synthesis*. (Wiley-VCH, 2015).
2. Chen, Z.-M., Zhang, X.-M. & Tu, Y.-Q. Radical aryl migration reactions and synthetic applications. *Chem. Soc. Rev.* **44**, 5220-5245 (2015).

3. Zhang, X.-M., Tu, Y.-Q., Zhang, F.-M., Chen, Z.-H. & Wang, S.-H. Recent applications of the 1,2-carbon atom migration strategy in complex natural product total synthesis. *Chem. Soc. Rev.* **46**, 2272-2305 (2017).
4. Li, W., Xu, W., Xie, J., Yu, S. & Zhu, C. Distal radical migration strategy: an emerging synthetic means. *Chem. Soc. Rev.* **47**, 654-667 (2018).
5. Wu, X. & Zhu, C. Radical-Mediated Remote Functional Group Migration. *Acc. Chem. Res.* **53**, 1620-1636 (2020).
6. Wu, X., Ma, Z., Feng, T. & Zhu, C. Radical-mediated rearrangements: past, present, and future. *Chem. Soc. Rev.* **50**, 11577-11613 (2021).
7. Chirpich, T. P., Zappia, V., Costilow, R. N. & Barker, H. A. Lysine 2,3-aminomutase. Purification and properties of a pyridoxal phosphate and S-adenosylmethionine-activated enzyme. *The Journal of biological chemistry* **245**, 1778-1789 (1970).
8. Ballinger, M. D., Reed, G. H. & Frey, P. A. An organic radical in the lysine 2,3-aminomutase reaction. *Biochemistry* **31**, 949-953 (1992).
9. Zhao, L.-P. *et al.* Nonheme Fe 1,3-nitrogen migratases for asymmetric noncanonical amino acid synthesis (Jul, 10.1038/s41589-025-01953-w, 2025). *Nature Chemical Biology* **21**, 1829-1829 (2025).
10. Han;, O. & Frey, P. A. Chemical model for the pyridoxal 5'-phosphate dependent lysine aminomutases *J. Am. Chem. Soc.* **112**, 8982–8983 (1990).
11. Wu, Z., Ren, R. & Zhu, C. Combination of a Cyano Migration Strategy and Alkene Difunctionalization: The Elusive Selective Azidocyanation of Unactivated Olefins. *Angew. Chem. Int. Ed.* **55**, 10821-10824 (2016).
12. Wei, D. *et al.* Radical 1,4/5-Amino Shift Enables Access to Fluoroalkyl-Containing Primary β(γ)-Aminoketones under Metal-Free Conditions (vol 60, 202110583, 2021). *Angew. Chem. Int. Ed.* (2021).
13. Li, Y. *et al.* A Copper-Catalyzed Aerobic 1,3 -Nitrogen Shift through Nitrogen-Radical 4-exo-trig Cyclization. *Angew. Chem. Int. Ed.* **56**, 15436-15440 (2017).
14. Ye, C.-X., Shen, X., Chen, S. & Meggers, E. Stereocontrolled 1,3-nitrogen migration to access chiral α-amino acids. *Nat. Chem.* **14**, 566–573 (2022).
15. Nie, X. *et al.* Nitrene-Mediated Enantioselective Intramolecular Olefin Oxyamination to Access Chiral γ-Aminomethyl-γ-Lactones. *Angew. Chem. Int. Ed.* **62** (2023).
16. Hong, Y. *et al.* Radical 1,2-Nitrogen Migration Cascades of β-Bromo α-Amino Acid Esters to Access β-Amino Acid Motifs Enabled by Cooperative Ni/Diboron Catalysis. *ACS Catal.* **14**, 5491-5502 (2024).
17. Liao, Z. *et al.* Asymmetric synthesis of β-amino acid derivatives by stereocontrolled $C(sp^3)$-$C(sp^2)$ cross-electrophile coupling via radical 1,2-nitrogen migration. *Nat. Commun.* **16** (2025).
18. Ren, X., Qiao, Y., Zhou, B., Liu, S. & Huang, Y. Nickel-catalysed enantioselective migratory reductive cross-coupling enabled by radical 1,2-amino migration. *Nat. Synth.* **4**, 1232-1246 (2025).
19. Hu, S.-P. *et al.* Integrating Olefin Carboamination and Hofmann-Löffler-Freytag Reaction by Radical Deconstruction of Hydrazonyl N-N Bond. *Angew. Chem. Int. Ed.* **63** (2024).
20. Fan, W. *et al.* Biomimetic 1,2-amino migration via photoredox catalysis. *Nat. Chem.* **17** (2025).
21. Wang, Q.-Z., Zheng, Y., Wu, W.-T. & Huang, H.-M. Oxa-π, σ-Methane Rearrangement Approach for Epoxide Synthesis. *J. Am. Chem. Soc.* **147**, 16248-16254 (2025).
22. Yuan, X.-Y., Wang, C.-C. & Yu, B. Recent advances in FeCl3-photocatalyzed organic reactions via hydrogen-atom transfer. Chin. Chem. Lett. 35, 109517 (2024).
23. Ding, L., Liu, Y., Niu, K. & Wang, Q. Photochemical alkynylation of hydrosilanes by iron catalysis. Chem. Commun. 58, 10679-10682 (2022).

24. Tu, J.-L., Hu, A.-M., Guo, L. & Xia, W. Iron-Catalyzed C(sp^3)-H Borylation, Thiolation, and Sulfinylation Enabled by Photoinduced Ligand-to-Metal Charge Transfer. J. Am. Chem. Soc. 145, 7600-7611 (2023).
25. Wellauer, J. et al. Rethinking the Excited-State Redox Properties of Iron(III) Complexes for LMCT Photoredox Catalysis. J. Am. Chem. Soc. 147, 29304-29314 (2025).
26. Eaton, M. C. et al. Caging the Chlorine Radical: Chemoselective Photocatalytic C(sp^3)-H Functionalization Enabled by Terminal Cu-Cl Sites in a Metal-Organic Framework. J. Am. Chem. Soc. 148, 1493-1502 (2026).
27. Kümper, M., Westermair, F. F., Götz, T., Gschwind, R. M. & Bauer, J. O. Si-H Activation via Dynamic Permutational Isomerism: A Ligand-Directed Route to Dehydrogenative Coupling. Angew. Chem. Int. Ed. 64, e202517017 (2025).
28. Rodríguez, A. M. et al. Introducing the Catalytic Amination of Silanes via Nitrene Insertion. J. Am. Chem. Soc. 144, 10608-10614 (2022).
29. Wu, J. et al. Palladium-catalyzed cascade of aza-Wacker and Povarov reactions of aryl amines and 1,6-dienes for hexahydro-cyclopenta[b]quinoline framework. Nat. Commun. 15, 6776 (2024).

Data availability: Experimental procedures and characterization data are available within this article and its Supplementary Information. Data is also available from the corresponding author on request.

Acknowledgments: The authors gratefully acknowledge the NSFC (Nos. 22267021), Yunnan Fundamental Research Projects (202401BF070001-021), Leading Talent Project of Innovation of Double Thousand Plan in Jiangxi Province (S2021DQKJ2195), Project of Innovative Research Team of Yunnan Province (202405AS350010). The authors also thank the Advanced Analysis and Measurement Center of Yunnan University for the sample testing service.

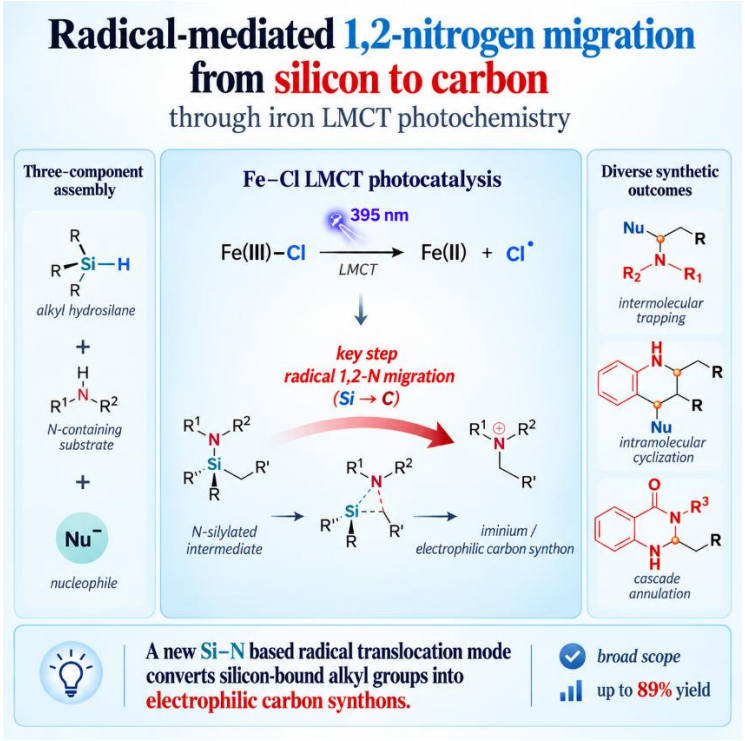
Author contributions: Y.J. and Y.Y. conceived and designed the experiments. Y.Y. performed the chemical experiments. Y.Y., H.J., S.W. and D.L. analyzed the data. Y.J., P.G. and Y.Y. wrote the manuscript. Z.S., Y.J. and P.G. supervised the project.

Competing interests: The authors declare no conflict of interest.

Additional information: All data are available in the main text or the supplementary materials. Additional data are available from the corresponding authors upon request.

Correspondence and requests for materials: should be addressed to P.G. (pg459@scarletmail.rutgers.edu) or Y.J. (jinyi@ynu.edu.cn).

Graphical Abstract



Supplementary Files

This is a list of supplementary files associated with this preprint. Click to download.

- CCDC2557203.cif
- checkcifCCDC2557203.pdf
- checkcifCCDC2559619.pdf
- CCDC2559618.cif
- checkcifCCDC2559618.pdf
- CCDC2559619.cif
- SINCYYY20260926.pdf